




Type 2 diabetic mice enter a state of spontaneous hibernation-like suspended animation following accumulation of uric acid

Received for publication, June 17, 2021, and in revised form, August 28, 2021 Published, Papers in Press, September 3, 2021,

<https://doi.org/10.1016/j.jbc.2021.101166>

Yang Zhao^{1,‡}, Rui Cheng^{1,‡}, Yue Zhao^{2,‡} , Wenhao Ge¹, Yunxia Yang¹, Zhao Ding¹, Xi Xu¹, Zhongqiu Wang³, Zhenguo Wu⁴, and Jianfa Zhang^{1,*}

From the ¹Center for Molecular Metabolism, Nanjing University of Science & Technology, Nanjing, China; ²Institute of Molecular and Cell Biology, Agency for Science, Technology and Research (A*STAR), Singapore; ³Affiliated Hospital of Nanjing, University of Chinese Medicine, Nanjing, China; and ⁴Division of Life Science, Hong Kong University of Science and Technology, Hong Kong, China

Edited by Qi-Qun Tang

Hibernation is an example of extreme hypometabolic behavior. How mammals achieve such a state of suspended animation remains unclear. Here we show that several strains of type 2 diabetic mice spontaneously enter into hibernation-like suspended animation (HLSA) in cold temperatures. Nondiabetic mice injected with ATP mimic the severe hypothermia analogous to that observed in diabetic mice. We identified that uric acid, an ATP metabolite, is a key molecular in the entry of HLSA. Uric acid binds to the Na⁺ binding pocket of the Na⁺/H⁺ exchanger protein and inhibits its activity, acidifying the cytoplasm and triggering a drop in metabolic rate. The suppression of uric acid biosynthesis blocks the occurrence of HLSA, and hyperuricemic mice induced by treatment with an uricase inhibitor can spontaneously enter into HLSA similar to that observed in type 2 diabetic mice. In rats and dogs, injection of ATP induces a reversible state of HLSA similar to that seen in mice. However, ATP injection fails to induce HLSA in pigs due to the lack of their ability to accumulate uric acid. Our results raise the possibility that nonhibernating mammals could spontaneously undergo HLSA upon accumulation of ATP metabolite, uric acid.

Hibernation is a survival strategy characterized by dramatic decreases in body temperature, heart rate, respiratory rate, and metabolism rate (1). Despite abnormal biochemical and physiological constraints, hibernators suffer no apparent injury due to a dramatic reduction in metabolic requirements (1, 2). Naturally hibernating animals generally increase their resistance to hypoxia and ischemia (3, 4) and are able to suppress the apoptotic response (5), maintain an immunosuppressed state to prevent general inflammation in the body, and survive a long period with no sign of organ damage (6, 7). The realization of human hibernation would have critical clinical applications, including reduced organ damage and long-term preservation of patients (8, 9).

Torpor and hibernation are traditionally defined as two different types of hypometabolic states under natural conditions (10). Different from torpor, animals under hibernation display much lower body temperatures and metabolic rates (11). A prominent physiologic and behavioral characteristic of hibernation is suspended animation, associated with tolerance to lethal metabolic rate reduction, bradycardia, and profound hypothermia (12). Some chemical compounds have been used to induce a hibernation-like suspended animation (HLSA) in nonhibernating animals. Hydrogen sulfide (H₂S) experimentally induces suspended animation in mice, and they will return to normal temperature after H₂S removal (13). However, H₂S has been reported to be toxic to the livers in both animals and humans (14). Another chemical, AMP, induces a reversible deep hypometabolic state in nonhibernating mice, which is assumed to be caused by increased blood 2,3-bisphosphoglycerate and inhibited binding of oxygen to red blood cells (15). In nature, the decline in body temperature is closely related to the adenosine signal of A₁ receptor in the brain (16). The central inhibition of A₁ receptor in the brain reverses the temperature rise of ground squirrels during hibernation, indicating that adenosine could play an essential role in adjusting body temperature (16).

The physiological definition of hibernation is not yet clear. During natural hibernation, glucose metabolism *via* glycolysis seems to be strongly suppressed. Inhibition of glycolysis readily induces hypothermia in a classic hibernator, indicating that the underlying mechanism of hibernation could be metabolic suppression (17). Indeed, the ability to replicate this naturally hibernating status has been achieved using metabolic inhibitors alone in rodents such as mice and rats (18). Insulin resistance is significant in the fattening period of hibernating animals. During the prehibernation period, serum insulin levels are elevated and maintain a high level in the initial months of hibernation (19). The actions of chronically high insulin levels are usually associated with insulin resistance in type 2 diabetes (T2DM). Lack of insulin response has also been reported in hibernating dormice and hedgehogs (20, 21). These observations imply there may be some similar metabolic

[‡] These authors contributed equally to this work.

* For correspondence: Jianfa Zhang, jfzhang@mail.njust.edu.cn.

Diabetic mice enter hibernation-like suspended animation

regulation mechanisms between type 2 diabetic mice and hibernating animals.

Here, we found that several strains of type 2 diabetic mice spontaneously enter into a hibernation-like suspended animation in cold temperatures. Nondiabetic mice with ATP injection mimic the severe hypothermia state similar to that observed in the type 2 diabetic mice. We identified that the accumulation of uric acid from ATP metabolism is an indispensable step in the induction of HLSA. Uric acid is an inhibitor of Na^+/H^+ exchanger, which controls the pH homeostasis of cytoplasm and influences the activities of a series of metabolic enzymes. It is well known that uric acid accumulation is a common feature of animals in long-term food shortage or fasting (22–25), and natural hibernation always commences when food is absent or limited (10). Our results strongly suggest that uric-acid-regulated metabolic suppression reflects not only a drop of metabolic activity during the development of T2DM, but also associates the metabolic regulation mechanism of natural hibernation.

Results

HLSA of the type 2 diabetic mice

Severe hypothermia observed during hibernation is a form of suspended animation (26). Accumulated evidence indicates that metabolic suppression must be a key factor to achieve hibernation (26). Hypometabolic behavior is also the main feature of T2DM. Therefore, we undertook a study to determine whether there were differential responses in body temperature (T_b) and locomotive activity while type 2 diabetic mice with severe metabolic stress were exposed to cold temperatures. Dramatically, the *db/db* diabetic mice displayed none of the thermoregulatory defenses when maintained in the environment with ambient temperatures (T_a) around the freezing point (0 °C). T_b measurement revealed a rapid decline accompanied by distinct behavioral responses with physical inactivity (Fig. 1A, left). About 1–3 h (stage I) after cold exposure, T_b of mice dropped to 18 ± 0.5 °C, and mice entered HLSA. In this stage, mice lost the righting reflex when placed on their backs or sides. The HLSA in type 2 diabetic *db/db* mice would last for several hours by adjusting the T_a of 17 ± 0.5 °C (stage II). Then, mice would arouse from HLSA spontaneously or be awakened when T_a was adjusted to more than 32 °C. This stage would last for about 2–3 h until the T_b of mice was close to 36 to 37 °C, and the moving activity was recovered (stage III). Simultaneously, the T_b in control mice was within the normal range. These differences were confirmed by surface thermal imaging (Fig. 1A, right).

The same HLSA has also been observed in HFD-STZ diabetic mice, while chow-fed lean control mice maintained a relatively constant T_b (Fig. 1B). Similarly, diabetic *ob/ob* mice entered into HLSA in cold temperatures, while nondiabetic *ob/ob* mice tended to reduce T_b and failed to enter into HLSA (Fig. 1C). During the HLSA in diabetic *ob/ob* mice, the average heart rate and respiratory rate also declined to about 69 beats per minute and 18 times per minute, respectively (Table 1). Moreover, all groups of type 2 diabetic mice showed a severe

decrease in spontaneous locomotive activity compared with control mice (Fig. 1, D–F). While oxygen consumption was relatively stable in control mice in cold temperatures, all type 2 diabetic mice decreased oxygen consumption accompanied by the drop in T_b (Fig. 1, G–I). These observations indicated that laboratory type 2 diabetic mouse models are capable of entering a suspended animation state similar to that observed in hibernators.

ATP induces HLSA in mice

The above observations could be explained by a changed metabolite that acted as a metabolic repressor in type 2 diabetic mice. We reasoned that the putative metabolic repressor, when injected into wild-type mice under cold exposure, should induce HLSA as observed in diabetic mice. Then we investigated whether endogenous energy molecules in diabetic mice were different from those in nondiabetic mice. HPLC analysis revealed that ATP metabolites, including hypoxanthine, xanthine, and uric acid, were elevated in the plasma and livers of diabetic *ob/ob* mice compared with nondiabetic *ob/ob* mice (Fig. 2, A–D). We hypothesized that the changes in endogenous energy molecules must be a key factor to achieve HLSA in diabetic mice.

Therefore, we undertook a study to determine whether there were differential responses in T_b while administrating endogenous energy molecules in animals. The wild-type mice were given adenosine triphosphate (ATP 2Na salt) and then maintained at 4 °C of T_a . They displayed no thermoregulatory defenses as observed in diabetic mice under cold exposure. T_b measurement revealed a rapid decline accompanied by distinct physical inactivity (Fig. 2E). About 30 min (stage I) after ATP injection, T_b dropped to 16 ± 0.5 °C, and mice entered the HLSA (stage II). T_b drop caused by ATP was clearly detected with an infrared thermometer (Fig. 2F), and a severe decrease of locomotive activity compared with control mice was measured by a radio frequency receiver platform (Fig. 2G). HLSA would last for about 6–8 h. Then, mice would arouse from HLSA spontaneously or be awakened when T_a was adjusted to 25 °C, and the moving activity was recovered (stage III). The changes in oxygen consumption corresponded with the major decline in T_b (Fig. 2H). During the HLSA in mice, the average heart rate and respiratory rate also declined to about 85 beats per minute and 13 times per minute, respectively (Table 2). The concentrations of ATP are important for entering HLSA. With the increase of ATP dosage, the entry time of HLSA was shortened (Fig. 2I). Together, these studies showed that ATP is a signaling molecule that can activate HLSA, which is used as a mechanism for energy conservation.

ATP-induced HLSA is independent of purinergic receptors

Next, we compared the effects of ATP and its downstream products, AMP and adenosine, on the induction of hypothermia. At a T_a of about 4 °C, ATP induced 100% of mice to HLSA, while AMP and adenosine were about 80% and 60%, respectively (Fig. 3A). The HLSA entry time of ATP was shorter than that of AMP and adenosine (Fig. 3B). In order to

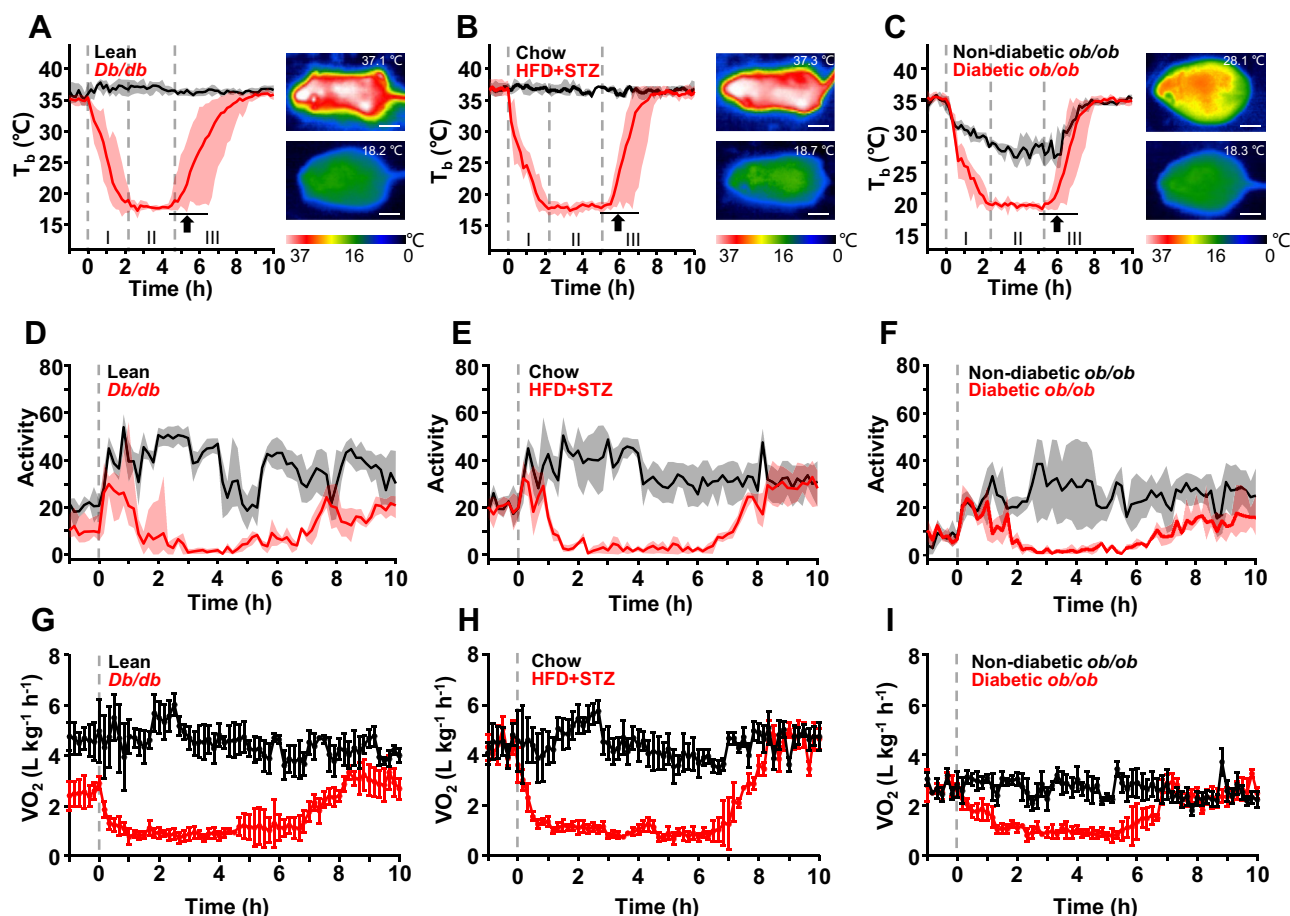


Figure 1. Cold exposure induces a hibernation-like suspended animation in diabetic mice but not in nondiabetic mice. *A*, simultaneous measurements of body temperature (T_b) in *db/db* mice or lean mice after cold treatment. Data were presented as mean \pm range ($N = 6$). Thermal images showing surface temperature difference at 3 h after cold treatment. The *dashed line* represents the division between stages. Scale bar: 2 cm. Stage I: induction stage; Stage II: maintenance stage; Stage III: awakening stage. *B*, simultaneous measurements of T_b in mice fed chow or mice fed HFD and treated with STZ after cold treatment. Data were presented as mean \pm range ($N = 6$). Thermal images showing surface temperature difference at 3 h after cold treatment. Scale bar: 2 cm. *C*, simultaneous measurements of T_b in diabetic mice or nondiabetic *ob/ob* mice after cold treatment. Data were presented as mean \pm range ($N = 6$). Thermal images showing surface temperature difference at 3 h after cold treatment. Scale bar: 2 cm. *D–F*, gross motor activity between *db/db* mice and lean mice (*D*), HFD-STZ mice and chow-fed control mice (*E*), diabetic *ob/ob* mice, and nondiabetic *ob/ob* mice (*F*). The *dashed line* indicates cold exposure onset. *G–I*, O_2 consumption between *db/db* mice and lean mice (*G*), HFD-STZ mice and chow-fed control mice (*H*), diabetic *ob/ob* mice, and nondiabetic *ob/ob* mice (*I*). The *dashed line* indicates cold exposure onset. Data were presented as mean \pm SD ($N = 6$).

determine whether the specific role of ATP was performed by its receptor P_2X or P_2Y , we used the antagonists of P_2X and P_2Y . While P_2X antagonist pyridoxalphosphate-6-azophenyl-2',4'-disulfonic acid (PPADS) had no effect on the induction of ATP, the antagonist of P_2Y receptor suramin significantly prolonged the induction period of ATP (Fig. 3C). However, no matter how high the dose of suramin is, it could not completely block mice from ATP-induced HLSA.

Plasma ATP can be rapidly degraded to ADP, AMP, and then adenosine. To investigate whether ATP induces HLSA *via* the adenosine receptors, ATP was administered to mice deficient in A_1 , A_{2a} , A_{2b} , and A_3 adenosine receptors, respectively. Figure 3D showed that ATP induced HLSA in all adenosine receptor knockout mice. Next, we detected that the metabolites of ATP were elevated in the plasma and livers of ATP-treated mice at 1 h after the injection. As observed in type 2 diabetic mice, ATP led to the accumulation of a large number of intermediate and terminal metabolites, including hypoxanthine, xanthine, and uric acid, in the plasma and livers

of mice (Fig. 3, E–H). These data implied that the accumulations of ATP metabolites might play a role in ATP-induced HLSA.

ATP metabolites acidify cytoplasm

Because ATP-induced hypothermia is immediate, we reasoned that ATP action in this process was very fast, and it could not be achieved through complex regulation of gene and protein expression, although some of them may have a rapid

Table 1
Changes in heart rate and respiratory rate in nondiabetic *ob/ob* mice and diabetic *ob/ob* mice after cold treatment

Group	Heart rate (bpm ^a)	Respiratory rate (bpm ^b)
Nondiabetic <i>ob/ob</i> ($N = 6$)	473 \pm 66	85 \pm 21
Diabetic <i>ob/ob</i> ($N = 6$)	69 \pm 11**	18 \pm 7**

Data were presented as mean \pm SD (Student's *t* test: ** $p < 0.01$).

^a Beats per minute.
^b Breaths per minute.

Diabetic mice enter hibernation-like suspended animation

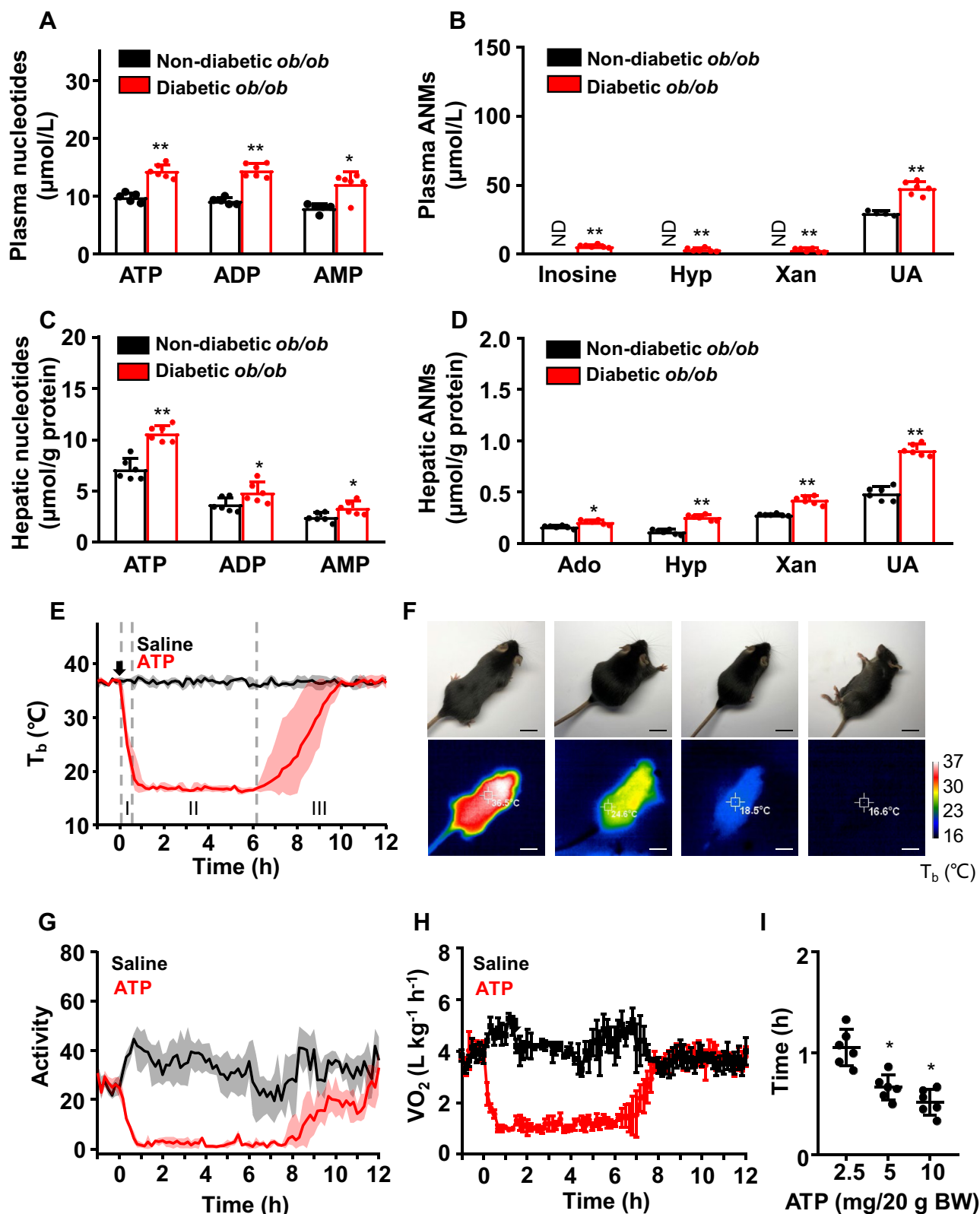


Figure 2. Elevated nucleotide levels in diabetic mice and ATP can induce HLSA in wild-type mice. *A* and *B*, quantification of adenine nucleotides (AN) and adenine nucleotide metabolites (ANMs) (*B*), including inosine, hypoxanthine (Hyp), xanthine (Xan), and uric acid (UA), in the plasma of diabetic *ob/ob* mice compared with nondiabetic *ob/ob* mice. Data were presented as mean \pm SD ($N = 6$; Student's *t* test: * $p < 0.05$, ** $p < 0.01$). *C* and *D*, quantification of adenine nucleotides (*C*) and ANMs (*D*), including adenosine (Ado), Hyp, Xan, and UA, in the liver of diabetic *ob/ob* mice, compared with nondiabetic *ob/ob* mice. Data were presented as mean \pm SD ($N = 6$; Student's *t* test: * $p < 0.05$, ** $p < 0.01$). *E*, Simultaneous measurements of T_b of mice given ATP (0.5 mg/g, i.p., indicated by a down arrow, red) or saline (black). Data were presented as mean \pm SD ($N = 6$). *F*, representative real-time photographs and digital infrared thermal images of mice after ATP injection. Scale bar: 2 cm. *G* and *H*, activity levels (*G*) and O_2 consumption (*H*) after injection of ATP or saline. Data were presented as mean \pm SD ($N = 6$). *I*, the entry time of HLSA induced by different ATP doses. Data were presented as mean \pm SD ($N = 6$; ANOVA: * $p < 0.05$).

Table 2
Changes in heart rate and respiratory rate in control mice and mice under HLSA state

Group	Heart rate (bpm ^a)	Respiratory rate (bpm ^b)
Control (N = 10)	552 ± 87	91 ± 13
HLSA (N = 10)	85 ± 8**	13 ± 5**

Data were presented as mean ± SD (Student's *t* test: ***p* < 0.01).

^a Beats per minute.

^b Breaths per minute.

response. Then, we investigated whether exogenous nucleotides immediately changed the metabolic environment, such as intracellular pH. Figure 4A showed representative pseudo-colored ratio images of intracellular pH value. The results revealed that ATP metabolites, including adenosine, hypoxanthine, xanthine, and uric acid, acidified cytoplasm with different efficiency, and uric acid is the most effective for cytoplasm acidification. Then, several metabolic enzymes would be impaired or lost their catalytic activity. Glucokinase and phosphofructokinase are two rate-limiting enzymes of glycolysis. The activities of these enzymes decreased with the decline of pH (Fig. 4, B and C). Fluorescence intensity assay revealed that glucose uptake was also significantly impaired with uric acid incubation in cultural cells (Fig. 4, D and E).

Since uric acid is the most effective inducer of intracellular acidification and the elevation in UA level and the decrease in body temperature occurred simultaneously (Fig. S1), we investigated whether the inhibition of uric acid accumulation influenced HLSA in mice. Xanthine oxidase is required to participate in the biosynthesis of uric acid. Surprisingly, when mice were pretreated with the inhibitors of xanthine oxidase, febuxostat, or allopurinol, ATP failed to induce mice to HLSA (Fig. 4, F and G), nor could diabetic *db/db* mice (Fig. S2). These pretreated diabetic mice lost the ability to enter stage II and recovered to normal T_b or died within 1–2 h during stage I. Moreover, mice pretreated with a uricase inhibitor potassium oxonate for 7 days developed hyperuricemia and could spontaneously enter into HLSA under cold exposure (Fig. S3). These studies indicated that uric acid suppresses metabolic rate by acidifying cytoplasm, and uric acid is indispensable during ATP-induced HLSA in mice.

Uric acid is an endogenous inhibitor of Na⁺/H⁺ exchanger

To identify the target of uric acid acidifying cell, the relationship between uric acid and the Na⁺/H⁺ exchanger activity was investigated. The Na⁺/H⁺ exchanger is a key regulator of cellular pH homeostasis. Interestingly, uric acid inhibited the activity of Na⁺/H⁺ exchangers in a dose-dependent manner. (Fig. 5, A–C). Na⁺/H⁺ exchanger 1 (NHE1) is one of the most important isoforms of Na⁺/H⁺ exchanger and is ubiquitously distributed throughout the plasma membrane of virtually all tissues. We investigated whether uric acid could interact with NHE1 proteins. The structure of the transmembrane segments of NHE1 was predicted according to *Phyre2* homology modeling portal. We then conducted the molecular docking by

AutoDock4.2 software. According to the molecular docking prediction, uric acid displayed a high binding affinity to the extracellular Na⁺-binding site of NHE1 protein, and the crucial amino acids involved in the NHE1-uric acid binding are SER161, PHE164, PHE165, and PHE467 (Fig. 5D). Then, knockout of the possible uric acid-binding domain (15 amino acid residues from position 156–170) was implemented by overlap extension PCR (Fig. 5E). A microscale thermophoresis assay verified that uric acid was able to bind to NHE1 (Fig. 5F). Nontransfected NIH3T3 cells were used to verify the absence of binding with a nonrelevant mCherry-fused protein, which was undetectable in undiluted lysates. The binding between NHE1 and uric acid was virtually abolished when this putative binding region was mutated (Fig. 5G).

Moreover, in the AML12 cells transfected with specific siRNA targeting NHE1, the initial pH_i value was decreased, and the decrease of pH_i triggered by uric acid was dampened (Fig. 5H, upper panel). The sequence-optimized NHE1-WT constructs, but not NHE1-mutant, rescued the effects of intracellular acidification reduced by NHE1-siRNA (Fig. 5H, middle and lower panels). Interestingly, the wild-type mice injected intravenously with zoniporide hydrochloride hydrate, a selective inhibitor of NHE1, were successfully induced into HLSA (Fig. S4). Together, these studies indicated that the primary role of uric acid is as an endogenous inhibitor of Na⁺/H⁺ exchanger.

Mice undergone HLSA have no systemic inflammation or organ damage

To determine whether the mice under HLSA or recovery from HLSA (R-HLSA) have systemic inflammation or organ damages, we evaluated plasma levels of MMP-1, IL-1β, and CRP by ELISA. There were no statistically significant differences in MMP-1, IL-1β, and CRP levels between the HLSA, R-HLSA, and control groups (Fig. 6A, upper left panel). In order to assess the heart, kidney, and liver functions, we measured the plasma levels of creatine kinase-MB (CK-MB), creatinine, blood urea nitrogen (BUN), aspartate aminotransferase (AST), and alanine aminotransferase (ALT) in all groups. Using plasma CK-MB as a marker of heart injury, we observed no significant increase in plasma CK-MB in the HLSA and R-HLSA groups compared with the control group (Fig. 6A, upper right panel). The levels of BUN and creatinine in plasma increased slightly in HLSA and dropped to the normal range in R-HLSA (Fig. 6A, lower left panel). It should be noted that the HLSA-mediated elevations in plasma AST and ALT compared with the control mice were small and likely represented no damage to liver tissue (Fig. 6A, lower right panel). Measurements of water and food consumption were performed 3 days before and 3 days after a single ATP-induced HLSA, respectively, and there was virtually no change (Fig. 6B, upper panel).

Then, we utilized metabolomics to investigate the metabolic changes in the circulation and main organs during and after HLSA. The PCA analysis was performed on the metabolic

Diabetic mice enter hibernation-like suspended animation

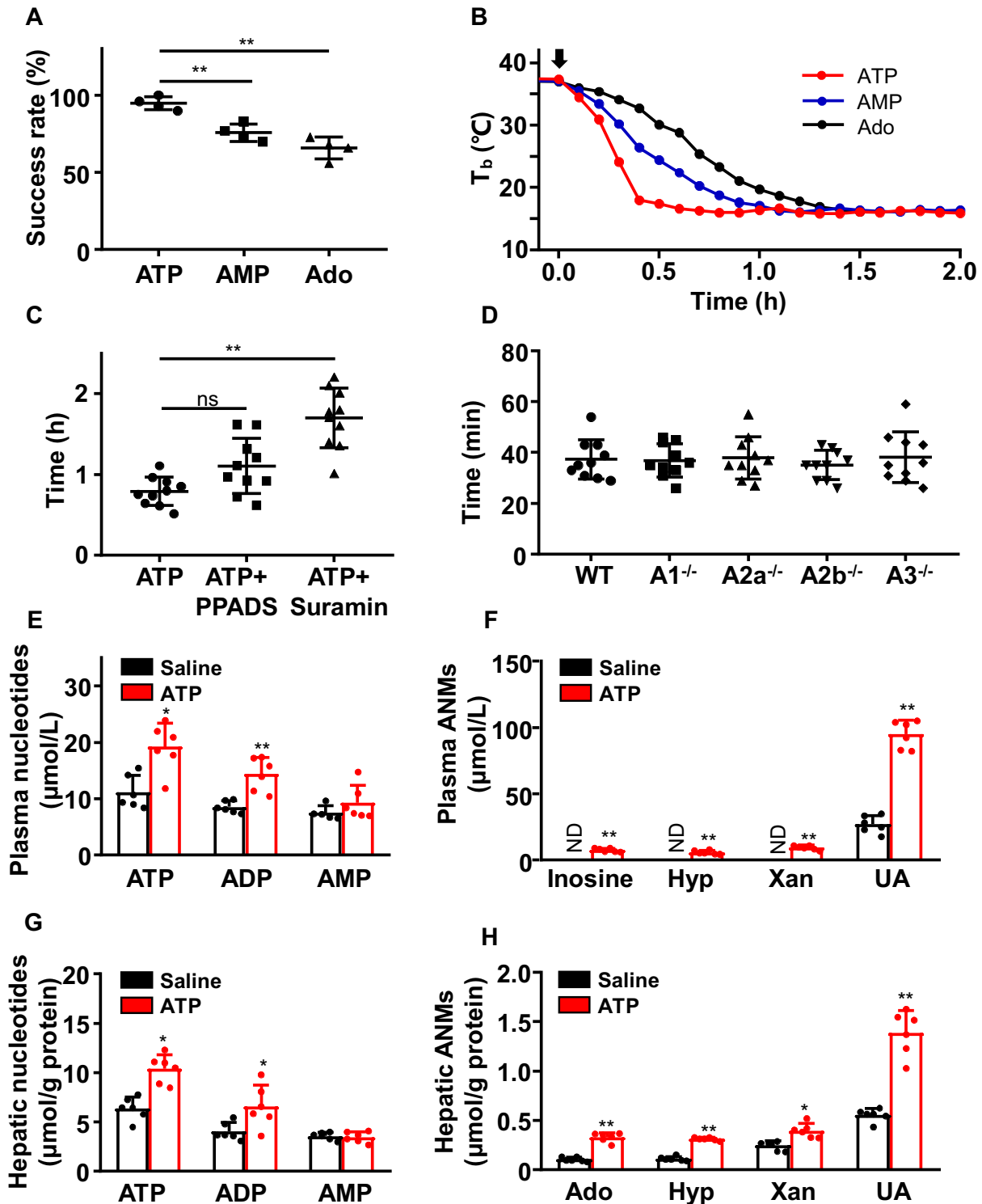


Figure 3. Purinergic receptor is not required in HLSA. *A*, different efficiency of ATP, AMP, and adenosine in inducing mice into the HLSA. Mice were injected with the same dose ($1 \mu\text{mol g BW}^{-1}$) of ATP, AMP, and adenosine, respectively, and were maintained at 4°C T_b . Data were presented as mean \pm SD from four time-independent experiments ($N = 20$ for each assay; ANOVA: $**p < 0.01$). *B*, simultaneous measurement of T_b of mice given ATP (red), AMP (blue), and adenosine (black) ($1 \mu\text{mol g BW}^{-1}$, indicated by down arrow) in individual metabolic chambers at $T_b \sim 4^\circ\text{C}$. *C*, the time of each stage of the hibernation-like state induced by ATP after using receptor antagonist of P_2X (suramin, 75 mmol/kg , i.p., 1 h before ATP-injection) or P_2Y (PPADS, 140 mmol/kg , i.p., 1 h before ATP-injection). Data were presented as mean \pm SD ($N = 10$; ANOVA: $**p < 0.01$). *D*, the time of each stage of the hibernation-like suspended animation induced by ATP in $A1^{-/-}$, $A2a^{-/-}$, $A2b^{-/-}$, and $A3^{-/-}$ mice. No significant differences in HLSA stages in these mice. Data were presented as mean \pm SD ($N = 10$; ANOVA: $p > 0.05$). *E* and *F*, quantification of adenosine nucleotides (*E*) and ANMs (*F*), including inosine, Hyp, Xan, and UA in the plasma of ATP-treated wild-type mice compared with saline-treated control mice at 1 h after the injection. Data were presented as mean \pm SD ($N = 6$; Student's *t* test: $*p < 0.05$; $**p < 0.01$). *G* and *H*, quantification of adenine nucleotides (*G*) and ANMs (*H*), including Ado, Hyp, Xan, and UA in the liver of ATP-treated wild-type mice compared with saline-treated control mice. Data were presented as mean \pm SD ($N = 6$; Student's *t* test: $*p < 0.05$; $**p < 0.01$).

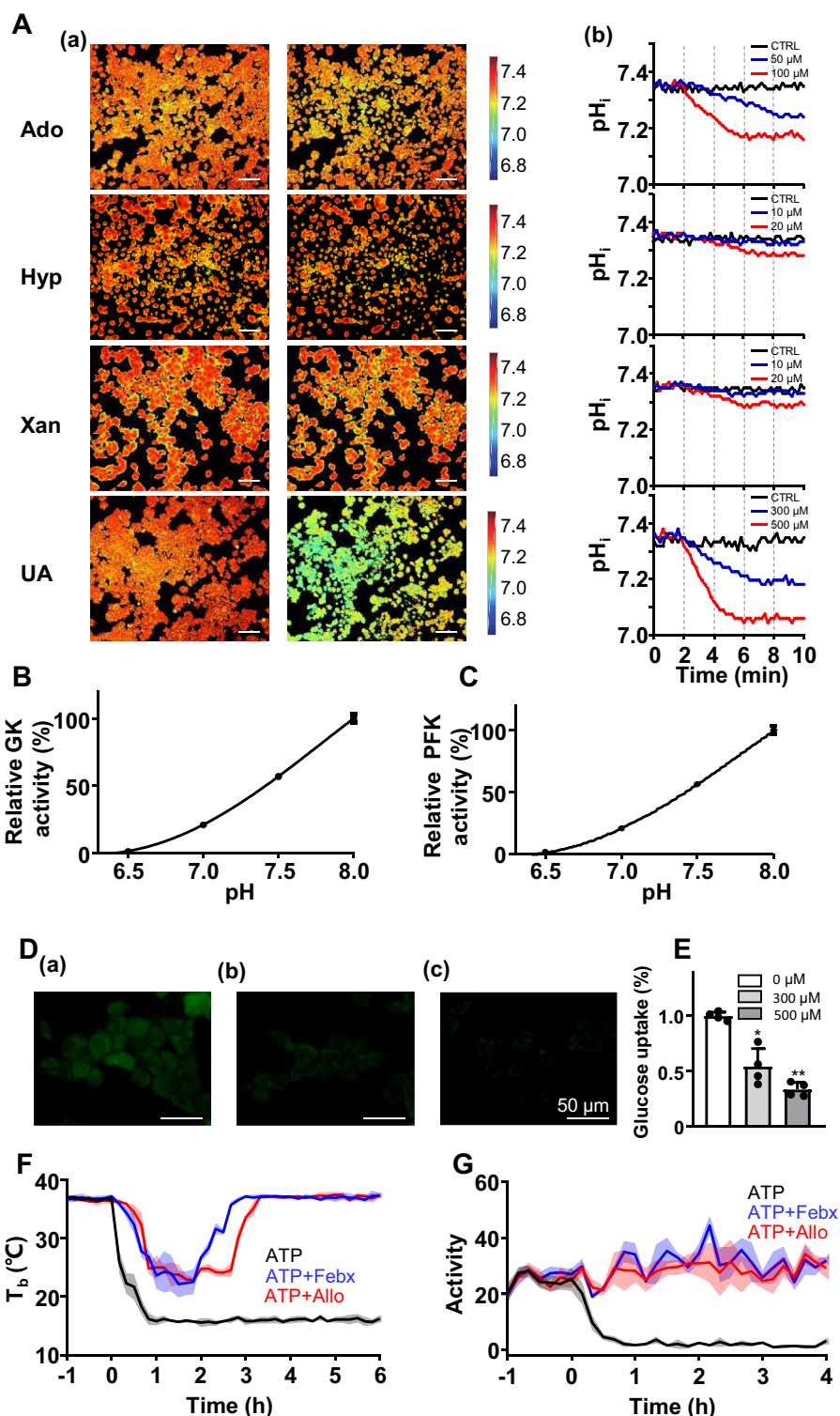


Figure 4. ATP metabolites immediately acidify the cytoplasm and UA is indispensable during ATP-induced HLSA. *A*, representative pseudo-colored ratio image showed a spatial map of intracellular pH (pH_i) (color pH scale to the right). *a*, the left and middle panels showed the difference of pH_i between cells treated with ATP metabolites (adenosine, hypoxanthine, xanthine, and uric acid) for 0 min (left) and 8 min (right), scale bar: 100 μm . *b*, the right panel showed a time course of change in pH_i after the addition of ATP metabolites. *B* and *C*, effect of the pH on the relative activity of glucokinase (*B*) and phosphofructokinase (*C*). Data were presented as mean \pm SD ($N = 5$ wells per treatment; note the error bars are smaller than the markers on the plot). *D*, representative images of AML12 at 0 μM UA (*a*), 300 μM UA (*b*), and 500 μM UA (*c*) for 30 min. Green fluorescence indicated the localization of glucose uptake by cells. Scale bar: 50 μm . *E*, glucose uptake in AML12 hepatocytes at 30 min after the addition of 300 μM or 500 μM UA measured by an FACSscan laser flow cytometer. Data were presented as mean \pm SD ($N = 6$ wells per treatment; ANOVA: * $p < 0.05$, ** $p < 0.01$). *F* and *G*, T_b changes (*F*) and activity level changes (*G*) after injection of ATP and xanthine oxidase inhibitors, febuxostat (5 mg/kg, i.p., 1 h before ATP-injection) or allopurinol (20 mg/kg, i.p., 1 h before ATP-injection). Data were presented as mean \pm SD ($N = 6$). Ado, adenosine; Allo, allopurinol; CTRL, control; Febx, febuxostat; POP, propionate; Hyp, hypoxanthine; UA, uric acid; Xan, xanthine.

Diabetic mice enter hibernation-like suspended animation

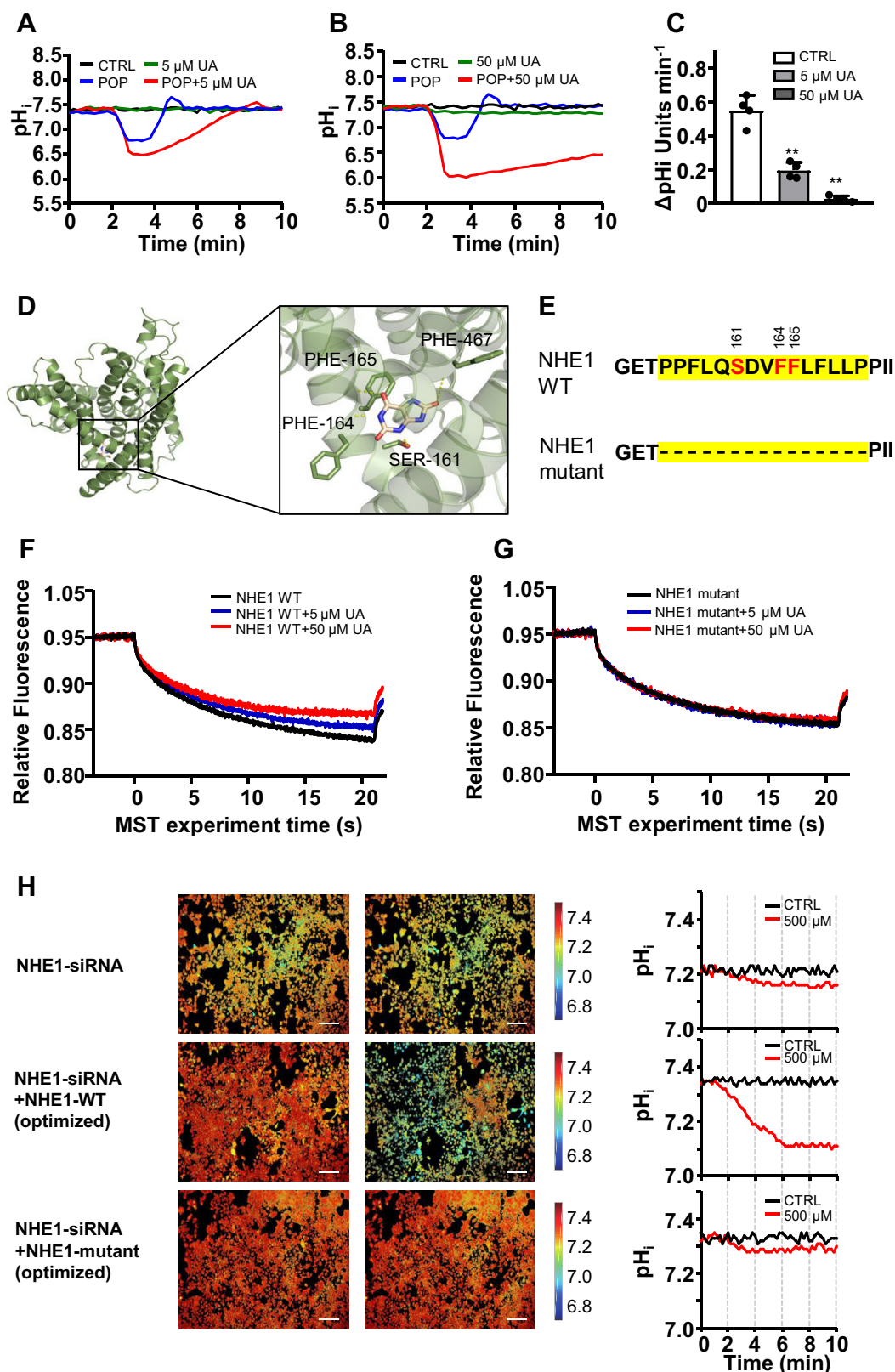


Figure 5. UA inhibits NHE1 activity and binds to the Na⁺- binding site of NHE1. *A* and *B*, effect of 5 μ M (*A*) or 50 μ M (*B*) UA on the recovery of pH_i from acidification induced by 20 mmol/l propionate. Original tracings of typical experiments for pH_i measurement were shown. *C*, Na⁺/H⁺ exchanger activity was rapidly reduced by 5 μ M UA and 50 μ M UA. Data were presented as mean \pm SD (N = 6; ANOVA: ***p* < 0.01). *D*, alignment of the docking poses and key residues in the NHE1 and UA complexes. *E*, schematic diagram of key amino acid residues knockout. *F*, MST time traces of two different concentrations of UA were mixed with NHE1-mcherry protein. *G*, MST time traces of two different concentrations of UA were mixed with NHE1-mcherry mutant protein. *H*, pseudo-colored ratio image showed a spatial map of intracellular pH (pH_i) (color pH scale to the right). The *left* and *middle* panels showed the difference of pH_i between cells treated with 500 μ M UA for 0 min (*left*) and 8 min (*right*). The *right* panel showed a time course of change in pH_i after the addition of UA. Scale bar: 200 μ m.

Diabetic mice enter hibernation-like suspended animation

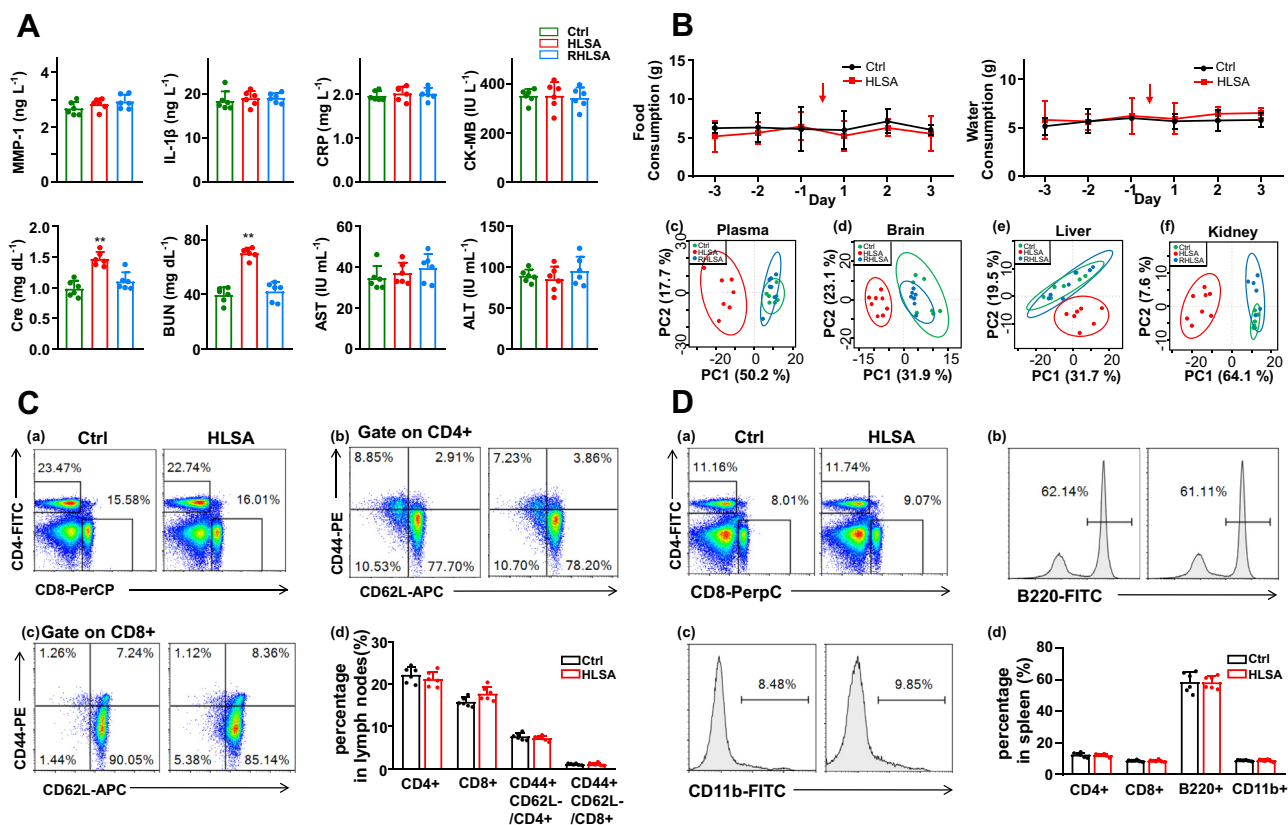


Figure 6. Assessments of organ damage and mouse metabolites during HLSA or recovery from HLSA. *A*, upper left panel, MMP-1, IL-1 β , and CRP levels in plasma had no significant change between the control group, HLSA group, and R-HLSA group. Upper right panel, CK-MB as a marker of heart injury in the plasma had no significant change between the control group, HLSA group, and R-HLSA group. Lower left panel, creatinine and BUN as markers of kidney injury in the plasma slightly increased in the HLSA group and returned to normal level after recovery from HLSA. Lower right panel, AST and ALT as markers of liver injury in the plasma showed no change between the control group, HLSA group, and R-HLSA group. Data were presented as mean \pm SD (N = 6; ANOVA: ** p < 0.01). *B*, upper panel, food consumption and water consumption 3 days before and 3 days after a single ATP-induced HLSA depicted no change. Data were presented as mean \pm SD (N = 6; ANOVA: p > 0.05). Lower panel, metabolomics analysis of scores plot from PCA analysis based on ^1H NMR data from the plasma, brain, liver, and kidney of the control group, HLSA group, and R-HLSA group. The PCA score showed clusters correspond to metabolic patterns in different groups, with each point representing one sample. Circles represent 95% confidence interval for each score in each group (see also Figs. S5–S8). *C*, draining lymph nodes of mice that underwent HLSA once a day for 10 consecutive days were analyzed with FACS. CD44 and CD62L were used to quantify the percentage of effector T cells. Upper left panel, flow cytometry quantification of CD4 $^+$, CD8 $^+$ T cells in draining lymph nodes. Upper right panel, representative flow cytometry analysis dot plot of effector CD4 $^+$ T cells (CD44 $^+$ CD62L $^-$ of total CD4 $^+$ T cells). Lower left panel, representative flow cytometry analysis dot plots of effector CD8 $^+$ T cells (CD44 $^+$ CD62L $^-$ of total CD8 $^+$ T cells) are shown. Lower right panel, the percentage of CD4 $^+$, CD8 $^+$ T cells, effector CD4 $^+$ T cells, effector CD8 $^+$ T cells. Data were presented as mean \pm SD (N = 6; Student's t test: p > 0.05). *D*, the spleens of mice that underwent HLSA once a day for 10 consecutive days were analyzed with FACS. B220 and CD11b were used to quantify immune cell populations. Upper left panel, flow cytometry quantification of CD4 $^+$, CD8 $^+$ T cells in spleens. Upper right panel, representative flow cytometry analysis dot of B cell (B220 $^+$) populations in the spleens. Lower left panel, representative flow cytometry analysis dot of effector CD11b $^+$ T cells was shown. Lower right panel, the percentage of CD4 $^+$, CD8 $^+$ T cells, B cells, and CD 11b $^+$ cells. Data were presented as mean \pm SD (N = 6; Student's t test: p > 0.05). Cre, creatinine; Ctrl, control group; HLSA group, hibernation-like suspended animation; R-HLSA group, mice recovered from hibernation-like suspended animation.

profiles of the control, HLSA, and R-HLSA groups. In the PCA score plots from the plasma, liver, kidney, and brain (Fig. 6B, lower panel), the HLSA group was well separated from the control group, while the R-HLSA group and control group clustered together, revealing that with the recovery of T_b , mice can quickly recover from HLSA-induced metabolic disturbance without apparent damage. The corresponding coefficient-coded loading plots (Figs. S5–S8) also elucidated that mice could quickly recover from HLSA-induced metabolic disturbance to their normal status.

To observe the influence of the ATP-induced HLSA on the immune system, flow cytometric analysis of the draining lymph nodes and spleens was performed after mice underwent HLSA once a day for 10 consecutive days. There was no

change in the percentages of immature T cells in the lymph nodes (Fig. 6C) and the spleens (Fig. 6D). Together, these results demonstrated that ATP-induced HLSA has no systemic inflammation or organ damage.

ATP induces HLSA in rats and dogs

Next, we investigated the effects of ATP in other mammals. Rats were injected with ATP and then maintained at a T_a of about 4 $^{\circ}\text{C}$. The behavior response of rats during HLSA was similar to that observed in mice. However, the time of entering HLSA is about 2.5–3 h (stage I) in rats, compared with 0.5 h in mice (Fig. 7A). The T_b of rats in HLSA was close to 16 $^{\circ}\text{C}$, as same as that of mice. Then, we transferred these rats to a T_a of

Diabetic mice enter hibernation-like suspended animation

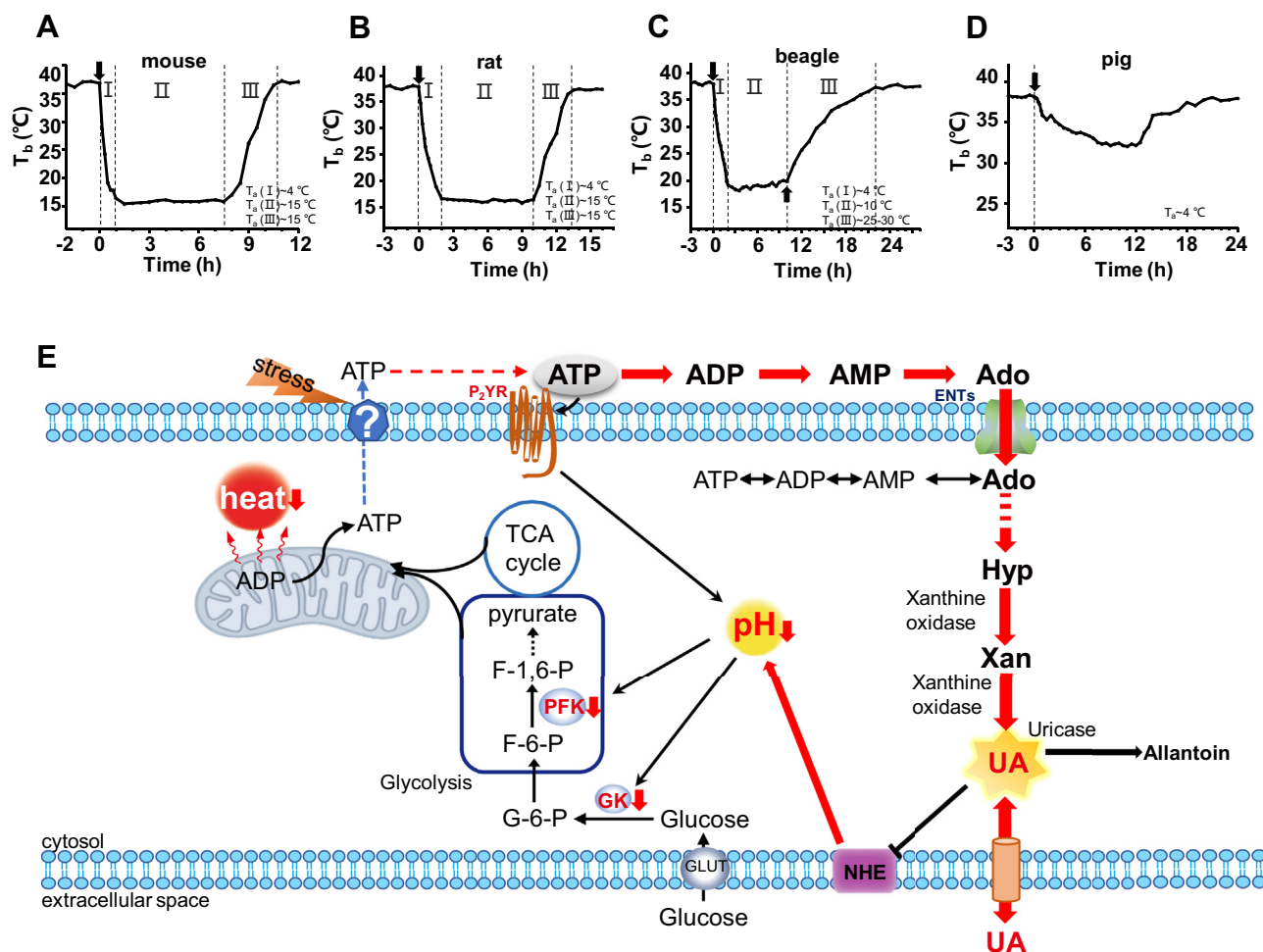


Figure 7. ATP induces HLSA in mice, rats, and beagles, but not in pigs. *A*, representative curve of T_b changes in mice after ATP injection (1 $\mu\text{mol/g}$ BW). The *dashed line* represents the division between stages. Stage I: induction stage; Stage II: maintenance stage; Stage III: awakening stage. *B*, representative curve of T_b changes in rats after ATP injection (1 $\mu\text{mol/g}$ BW). Rats were shaved off prior to ATP injection. Rats can awaken spontaneously undergoing stage II for 6–8 h. *C*, T_b changes in beagles after ATP injection (0.5 $\mu\text{mol/g}$ BW). Beagles were shaved off prior to ATP injection. During stage II, the beagles were unable to awaken spontaneously until they were transferred to room temperature. *D*, T_b changes in pigs after ATP injection (0.5 $\mu\text{mol/g}$ BW). Pigs only declined their T_b to 32–33 °C and remained active for several hours. The *dashed line* indicates cold exposure onset. *Down arrow* indicates injecting time points, and *up arrow* indicates transferring time points. *E*, schematic representation of the proposed regulatory function of ATP on the induction of an HLSA. The model shows ATP causes UA accumulation, thereby acidifying the cytoplasm and inhibiting the production of heat from glucose oxidation phosphorylation.

about 15 °C. The rats would keep HLSA for 6–8 h (stage II). The rats were then awakened by being moved to a T_a of 25 °C. After 3–4 h (stage III), the T_b of the rats would recover to close to 37 °C (Fig. 7B). The time of stage III in mice is about 2–3 h. The rats in stage II could also awaken by elevating T_a at any required time. For dogs, they must be shaved off prior to ATP injection. Shaved dogs were injected with ATP and maintained at a T_a of about 4 °C (Fig. 7C). After 1.5–2 h (stage I), the dogs would enter the HLSA similar to that observed in rats and mice. The T_b of dogs in HLSA was about 18–20 °C. Then, we transferred the dogs to a T_a of 10 °C. The dogs could maintain HLSA for 8–10 h (stage II). The dogs during stage II could not spontaneously arouse at T_a of 10 °C. However, while the dogs were transferred to a T_a of 25–30 °C, their T_b would recover to about 37 °C within 8–10 h (stage III, Table S1). Especially, when injected with ATP (0.5 $\mu\text{mol/g}$ BW) intraperitoneally at 4 °C, the pigs only reduced their T_b to 32–33 °C and remained active for several hours (Fig. 7D). Pigs injected with ATP

(1 $\mu\text{mol/g}$ BW) at 4 °C would die within 8–12 h. ATP could not induce pig to HLSA.

Discussion

Type 2 diabetes and hibernation are two different pathological and physiological phenomena. However, both of them have a common metabolic characteristic that glucose utilization is seriously inhibited. Hibernators are considered a remarkable model for reversible insulin resistance (27). Many hibernators naturally undergo a massive increase in body fat storage before the hibernation season and, to a large extent, rely on triglycerides in white adipose tissue as an energy source in winter (28, 29). For fat-storing hibernators, reduced metabolic rate and body temperature are also accompanied by shifts of fuel utilization and energy-generating pathways from the utilization of carbohydrates to the utilization of fat (26, 30, 31). In T2DM, the actions of chronically high insulin levels are

usually associated with insulin resistance, and metabolic reprogramming results in alterations in fuel utilization (32, 33). The uncoupling of glycolysis from glucose oxidation and increased fatty acid oxidation are considered specific metabolic changes of T2DM. Thus, there is a reasonable physiological and metabolic basis for type 2 diabetic animals to enter a spontaneous HLSA in cold temperatures.

Persistently elevated blood nucleotide levels and constant purinergic signaling may play a pathophysiological role in the development of T2DM (34). Analysis of the relationship between circulating nucleotide concentrations and clinical measures of T2DM demonstrate that changes in nucleotide metabolism are direct metabolic consequences of the disease and do not result from secondary complications (34). High nucleotide levels observed in some morbidly obese subjects seem to be associated with the initial stage of insulin resistance (35). Uric acid is the ultimate product of purine metabolism in the human body. A close association between serum uric acid and abnormal glycometabolism has been well built (36, 37). The current analyses suggest that elevated serum uric acid concentrations have been positively associated with the development of T2DM (37, 38). In our present study, uric acid is an inhibitor of Na^+/H^+ exchanger, which directly regulates cell pH homeostasis. Acidifying cell suppresses the metabolic rate through influencing a series of metabolic enzymes. The suppression of uric acid biosynthesis blocks the occurrence of HLSA in both type 2 diabetic mice and ATP-treated wild-type mice, suggesting a crucial role of uric acid in the induction of HLSA. On the other hand, ATP interaction with P_2 receptors to acidify cellular plasma also plays a partial role in the induction of HLSA. Thus, the entry time of ATP in inducing hibernation is shorter than that of AMP and adenosine. A previous investigation shows that pyruvate, an energy-rich metabolic intermediate, induces hypothermia in diet-induced obese mice (39), which relies on adenosine receptors and GABA signaling. Nevertheless, in our present ATP-induced HLSA, it seems adenosine receptor signaling is not a key trigger. Uric acid accumulation did not influence GABA levels in the cerebral hemisphere, cerebellum, and the medulla oblongata (40, 41). Several regions in the mammalian brain have been implicated in coordinating temperature regulation for the entrance into a hibernation-like state (42–44). While UA generally displays inhibitory effects of metabolism in peripheral tissues, it will be interesting to see whether it affects the thermoregulatory center in the brain.

The fact that ATP fails to induce pig to HLSA further supports our conclusion that higher levels of uric acid accumulation are essential in metabolic suppression. In pigs, uric acid is not a terminal product of ATP, and xanthine oxidase is required to participate in the production of uric acid, which is then metabolized to allantoin by uricase (45). The level of xanthine oxidase in pigs is very low, but the activity of uricase is quite high (46–49). Therefore, it is difficult to accumulate uric acid in pigs. Unlike uric acid, allantoin could not acidify cytoplasm (Fig. S9). In mice and rats, the levels of xanthine oxidase are thousands of times higher than that in pigs, and the levels of uricase are similar to that in pigs (46, 47, 50–52).

Thus, uric acid accumulates sharply following ATP injection in these animals. For humans and primates, uricase is absent in the evolutionary process. Uric acid is a final product from purine derivatives in humans and primates (53), indicating a possibility that ATP induces these large mammals into HLSA.

In natural hibernation, food shortage and reduced ambient temperature are two essential factors for entering an energy-conserving torpid state. For animals that have been deprived of food for a long time, their serum uric acid levels will increase (22). Plasma uric acid levels increased in fasting emperor penguins, accompanied by a lower level of locomotor activity (23). Spontaneously fasting birds increased their serum uric acid levels during migratory flight (24). It was reported that plasma levels of uric acid were increased in human undergoing 10 days of fasting (25), and increased urate in plasma has also been reported in hibernating bears and snakes (54, 55). Therefore, our results strongly suggest that uric-acid-modulated metabolic suppression may, at least in part, reflect a metabolic regulation mechanism during the early stage of natural hibernation when food is absent.

In summary, we uncover a mechanism of deep metabolic suppression (Fig. 7E) and describe a procedure for controlling suspended animation of nonhibernating mammals, including mice, rats, and dogs. The underlying mechanism of uric-acid-regulated metabolic suppression in T2DM is similar to that of natural hibernation. While humans are nonhibernators, the ability to undertake suspended animation could be preserved. Currently, mild hypothermia is an important clinical tool since cells have reduced metabolic activity and will survive longer under hypoxia stress (56). Potentially, severe hypothermia, as described here, could produce additional protection from hypoxia stress.

Experimental procedures

Experimental animals

We used male, 10–12-week-old C57BL/6 wild-type mice, *ob/ob* diabetic, and nondiabetic mice, C57BL/Ks *db/db* diabetic mice, and HFD-STZ-induced T2DM mice. Male adenosine receptor $\text{A1}^{-/-}$, $\text{A2a}^{-/-}$, $\text{A2b}^{-/-}$, and $\text{A3}^{-/-}$ mice aged 8–10 weeks were also used in this study. Male Sprague-Dawley rats were between 8 and 10 weeks old. Four Beagle dogs (two male/two female) aged 0.8–1 year and weighing 6.8–10 kg were included. Six pigs (three male/three female) aged 5–6 months weighing 15–20 kg were used. All animals were housed in a standard animal facility (ambient temperature, 22 °C–25 °C; relative humidity, 40%–60%) under a 12-h/12-h light/dark cycle and provided with standardized food and water. Mice or rats were housed two per cage unless otherwise specified. Beagle dogs or pigs were group-housed dependent on gender. All animal care and use procedures were approved by Institutional Animal Care and Use Committee at Nanjing University of Science and Technology (ACUC-NUST-20180012).

HLSA induction

For mice and rats, each animal was placed in an individual precooled cage with standard chow and water in a

Diabetic mice enter hibernation-like suspended animation

temperature-controlled chamber (LRH-500CL, Shanghai Yiheng Scientific Instrument Co, Ltd; 0 °C for type 2 diabetic mice and hyperuricemic mice, 4 °C for drug-induced nondiabetic mice and rats). The chamber temperature was immediately set at an appropriate temperature (17 °C for type 2 diabetic mice, 15 °C for nondiabetic mice or rats; heating rate: 8 °C/min) once the animals were losing righting reflex. For the recovery stage, animals can arouse spontaneously or under warm conditions (32 °C for type 2 diabetic mice, 25 °C for mice; heating rate: 8 °C/min). For beagles and pigs, each animal was first placed in an individual cage in a temperature-controlled ice room (4 °C). Once the beagles were losing righting reflex, the room temperature was immediately set at 10 °C. For the recovery of beagles, animals were removed to a warm animal facility (25–30 °C). Specially, the whole trunk hairs of rats and beagles were removed by electrical shaving with isoflurane anesthesia 2 days prior to the experiments. The shaved rats and beagles were remained on a heating pad and returned to their standard animal facility only after full recovery of body temperature and motor activity. All experiments started at about 8:00 AM and were performed under light illumination. Unsacrificed dogs and pigs were returned to the animal center to continue breeding.

Hyperuricemic model establishment

The mice hyperuricemic models were established as described previously (57). Briefly, C57BL/6 mice were injected intraperitoneally with potassium oxonate (Sigma, catalog no. 156124, 100 mg/kg) and inoculated orally with hypoxanthine (Sigma, catalog no. H9377, 600 mg/kg) at meantime for 7 consecutive days. HLSA induction was performed on the eighth day.

Measurements of core body temperature, heart rate, and respiratory rate

Core body temperatures were recorded with a rectal probe connected to a digital thermometer (BAT-12, Microprobe-Thermometer, Physitemp, NJ, US). Infrared images were recorded with an infrared camera (HT-18, Handheld-Infrared-Thermal-Imaging-Camera, Hti). Heart rates and respiratory rates were monitored *via* the Small Animal Physiological Monitoring System (75–1500, Harvard Apparatus Inc).

Measurements of locomotor activity and oxygen consumption

Locomotor activity and oxygen consumption were monitored using four VersaMax Animal Activity Monitors (AccuScan Instruments) combined with Fusion Metabolic System (AccuScan Instruments), each consisting of a Plexiglas chamber (40 cm × 40 cm × 30.5 cm). Plexiglas chambers were placed in a temperature-controlled chamber (LRH-500CL, Shanghai Yiheng Scientific Instrument Co, Ltd). A constant airflow (0.5 l/min) was drawn through the chamber and monitored using a metabolic monitor (AccuScan Instruments). The oxygen consumption rate was assessed at 10-min intervals.

Drug administration

ATP disodium salt hydrate (Sigma, catalog no. A1852), 5'-AMP sodium salt (Sigma, catalog no. A1752), and adenosine (Sigma, catalog no. A9251) were administered by intraperitoneal injection (1 μmol in PBS/g body weight). To study the role of P₂X and P₂Y receptor activation in ATP-induced HLSA, Suramin sodium salt (MCE, catalog no. HY-B0879A) and PPADS tetrasodium (MCE, catalog no. HY-101044) were injected intraperitoneally 1 h prior to ATP treatment. (suramin sodium salt, 75 mmol in PBS/kg; PPADS tetrasodium, 140 mmol in PBS/kg). To study the role of uric acid accumulation in HLSA, allopurinol (MCE, catalog no. HY-B0219, 20 mg/kg) or febuxostat (Beyotime Biotechnology, catalog no. SF1114, 5 mg/kg) was injected intraperitoneally 1 h prior to ATP treatment. For *db/db* diabetic mice, allopurinol (20 mg/kg) or febuxostat (5 mg/kg) was injected intraperitoneally for 4 consecutive days, then exposed to the cold 1 h after the last injection. Allopurinol and febuxostat were dissolved in DMSO, diluted in sterile saline to a final value of DMSO <10%. To study whether the inhibitor of NHE1 can induce HLSA, zoniporide hydrochloride hydrate (MCE, catalog no. HY-105064D, 4 mg/kg) was injected *via* the tail vein, and then mice were exposed to cold.

Tissue and blood sampling

Mice were euthanized by cervical dislocation. Blood was collected from the carotid arteries in anticoagulant tubes containing a stop solution (0.2 mmol/l dipyrindamole, 5 mmol/l erythro-9-(2-hydroxy-3-nonyl)-adenine, and 4.2 mmol/l EDTA) (58). Then organs were removed and freeze-clamped in liquid nitrogen within 5 s. Blood samples were immediately centrifuged at 3000g for 5 min at 20 °C. The plasma samples obtained were and then stored on ice and immediately used in the experiments.

HPLC analysis of nucleotides and the metabolites

Mouse organs and the plasma samples were homogenized using ice-cold 0.4 mol/l perchloric acid. Samples were analyzed using HPLC (Waters 1525 System; Millipore) on a reversed-phase C18 column as described previously (58, 59). The mobile phases are Buffer A (150 mM KH₂PO₄, 150 mM KCl, pH 6.0) and Buffer B (150 mM KH₂PO₄, 150 mM KCl, 15% acetonitrile, pH 6.0). Pure nucleotides and metabolites were used to identify the peaks and obtain the calibration curves. Nucleotides and their metabolites were quantitated based on the peak area compared with a standard curve and normalized to the protein content of frozen tissues.

Cell culture

AML12 cell lines were cultured in DMEM/F12 medium (Gibco) supplemented with 10% fetal bovine serum (FBS) (Gibco), 1% Insulin-Transferrin-Selenium (Gibco), 40 ng/ml dexamethasone (Sigma Aldrich), and 1% penicillin-streptomycin under humidified and 5% CO₂ conditions. NIH3T3 cell lines were cultured in DMEM medium (Gibco) supplemented with 10% fetal bovine serum (FBS) (Gibco) and

1% penicillin-streptomycin under humidified and 5% CO₂ conditions.

Glucose uptake

Glucose uptake assay was performed by using 2-NBDG (60). Briefly, Aml12 cells seeded in 24-well were treated with ATP. Then the medium was removed. The wells were added 2-NBDG (100 mg/ml) in a serum-free low glucose DMEM medium for 20 min at 37 °C. The cells were examined, and photographs were obtained with a fluorescence microscope (Nikon). The fluorescence intensity of 2-NBDG was recorded in the FL1 channel by using a FACScan laser flow cytometer (NovoCyte). Data from 10,000 single-cell events were collected.

Intracellular pH measurement

The measurements of intracellular pH (pH_i) were performed as previously described, with modification (61). AML12 cells were used and stained with Hanks' buffered saline solution (HBSS) solution containing 1 μmol/l (2',7'-bis-[carboxyethyl]-5-[and-6]-carboxyfluorescein)-tetraacetoxymethyl ester (BCECF-AM) for 20 min at 37 °C, and then rinsing the cells three times with dye-free solution. Then the cells were perfused with HBSS, and chemicals were added *via* a whole chamber perfusion system (KSX-Type1, Tokai Hit Co). pH_i measurements were performed at 37 °C using a fluorescence microscope (Nikon). BCECF fluorescence was excited at 490 nm and 440 nm, and emitted fluorescence was measured at 530 nm. The F490/F440 emission ratio was converted to a pH scale according to the nigericin technique.

Detection of Na⁺/H⁺ exchanger activity

AML12 cells were acidified with 20 mmol/l propionate replacing 20 mmol/l NaCl (62). The solutions used in the Na⁺/H⁺ exchanger activity measurements were composed of (in mM) as described earlier: NaCl 145, K₂HPO₄ 1.6, KH₂PO₄ 0.4, Ca-gluconate 1.3, MgCl₂ 1, and D-glucose 5; pH was adjusted to 7.4.

GK and PFK activity assays

GK and PFK activities in the liver extract were determined using a spectrophotometric enzymatic cycling assay kits (Solarbio) according to the manufacturer's instructions.

Homology modeling and docking

Human NHE1 (uniprot P19634, gene SLC9A1) secondary structure and transmembrane domain topology were predicted using *Phyre2* homology modeling portal (<http://www.sbg.bio.ic.ac.uk/phyre2>) as described previously (63). The resulting model of NHE1 with PDB 4CZB as a template comprised amino acids 100–500, which is the transmembrane domain that contains 12 transmembrane helices. *Autodock* software (*AutoDock* 4.2) was used to perform protein compound docking analysis. Docking grid boxes were first set as the

complete model of the NHE protein. Docking results indicate that UA is bound inside the Na⁺ binding pocket. The compounds were redocked with the specific binding to the Na⁺ binding pocket in order to achieve a more precise docking result. Molecular docking results were illustrated using the *PyMol* molecular graphic program.

mCherry-NHE1 constructs and fragment knockout

The sequence for the human NHE1 (uniprot P19634, gene SLC9A1) protein was obtained from *Uniprot*. DNA sequence was cloned into the pmCherry-N1 vector using the appropriate restriction sites with kanamycin resistance genes. The knockout of the possible UA-binding domain (15 amino acid residues from position 156–170) was generated by overlap extension PCR. The PCR primers were as follows: NHE1P1-F-EcoRI: GAA TTC GCC ACC ATG GTG CTG CGC A; NHE1P1-R: TAG CCG GCG TCC AGA ATA ATA GGT GTC TCG CCC ACG CCC TTG ATG A; NHE1P2-F: TCA TCA AGG GCG TGG GCG AGA CAC CTA TTA TTC TGG ACG CCG GCT A; NHE1P2-R-BamHI: TTA AGG ATC CCG AGA GCC TCC TCC. Mutant constructs were confirmed by DNA sequence analysis.

Membrane protein preparation and MST analysis

pmCherry-N1 plasmids encoding NHE1 or NHE1 mutant were transfected into NIH3T3 cells using *Lip2000* transfection kit (Invitrogen) according to the manufacturer's protocol. Transfected cells were harvested 48 h. The cell membrane protein extraction was performed according to the kit of Membrane and Cytosol Protein Extraction Kit (Beyotime Biotechnology, #P0033). MST experiments were performed on a Monolith NT.115 system (NanoTemper Monolith NT.115) using 20% excitation power and 90% MST-Power. Subsequently, 5 μl of membrane protein extraction was mixed homogeneously with 5 μl MST buffer dissolved with UA. After a short incubation, the samples were loaded into MST standard treated glass capillaries for MST analysis as described above. Each ligand-binding curve was measured at least three independently pipetted measurements.

NHE1 gene silencing and rescue

To knock down endogenous NHE1, Aml12 cells were transfected with siRNA-NHE1 using Lipofectamine 2000 agent (Invitrogen) as recommended by the manufacturer's guidelines. NHE1 knockdown was rescued by cotransfecting of the pcDNA3.1 plasmid carrying a sequence-optimized NHE1-WT or NHE1-mutant gene. Briefly, Aml12 cells were cultured in 35 mm dishes (3 × 10⁴ cells). Before transfection, cells were washed three times with PBS to remove any residual serum, and the medium was replaced with Opti-MEM (Gibco). siRNA or pcDNA3.1 was added in Opti-MEM and then mixed with Opti-MEM containing Lipofectamine 2000. The transfection complexes were directly added to each well. After 6 h of incubation, the medium containing transfection complexes was removed and changed with a fresh medium. Cells were further

Diabetic mice enter hibernation-like suspended animation

incubated for 48 h and stained for intracellular pH measurement.

Plasma biochemistry and cytokine assay

Plasma CK-MB, creatinine, BUN, AST, and ALT activities were measured by a spectrophotometric enzyme cycle assay kit (Jiancheng) according to the manufacturer's instructions. Serum MMP-1, IL-1 β , and CRP levels were measured by enzyme-linked immunosorbent assay (ELISA) kits (Boster Biological Technology Ltd) according to the manufacturer's protocol.

¹H NMR-based metabolomics analysis

Organ samples were extracted as previously described (64). ¹H NMR spectra of the samples were recorded on a Bruker AVANCE III 500-MHz spectrometer (Bruker) at 298 K. The ¹H NMR spectra of sample extracts were corrected for phase and baseline distortion and referenced manually by the same person to the TSP resonance at δ 0.00 using the TOPSPIN (V3.0, Bruker Biospin). Spectral regions δ 0.50–9.50 were automatically binned using a dynamic adaptive binning approach with equal width of 0.005 ppm. The noisy and residual water-affected regions were removed. The remaining spectral data was normalized by probabilistic quotient normalization (PQN) prior to pattern recognition analysis (65).

Flow cytometry

Flow cytometry was performed on draining lymph nodes and spleen. Single-cell suspensions were isolated from spleens and draining lymph nodes. Briefly, after underwent ATP-induced hibernation-like state once a day for 10 consecutive days, mice were sacrificed, and the whole spleen (about 80 mg) and draining lymph nodes (about 10 mg) were ground into small pieces, homogenized by a plastic pestle, and minced through sterilized meshes (200 meshes). Erythrocytes were lysed in a red blood cell lysis buffer (hypotonic ammonium chloride buffer). Approximately 100,000 harvested cells from draining lymph nodes and spleen. Conjugated monoclonal antibodies to mouse FITC rat anti-mouse CD4 Clone GK1.5 (eBioscience Cat#: 11-0041-82), PerCP-Cyanine5.5 rat anti-mouse CD8 Clone 53-6.7 (eBioscience Cat#: 45-0081-80), FITC rat anti-mouse CD11b Clone M1/70 (eBioscience Cat#: 17-0112-82), PE rat anti-mouse CD44 Clone IM7 (eBioscience Cat#: 12-0441-82), APC rat anti-mouse CD62 L Clone MEL-14 (Biolegend Cat#: 104412), FITC rat anti-mouse B220 Clone RA3-6B2 (eBioscience Cat#: 11-0452-82) were used. The analysis was performed by a NovoCyte flow cytometer (ACEA Bioscience Inc).

Statistical analysis

Statistical analysis between groups was performed as the following: *p* values were calculated using one or two-tailed Student's *t* test for pairwise comparison of variables; one-way analysis of variance (ANOVA) followed by Tukey's post hoc test for multiple comparisons of variables; two-way ANOVA

followed by Tukey's post hoc test for multiple comparisons involving two independent variables. *p* values: **p* < 0.05; ***p* < 0.01. All results with *p* < 0.05 were considered statistically significant. Sample sizes of all experiments were predetermined by calculations derived from our experience. No sample was excluded from the analyses. Animals were not randomly assigned during collection, but the strain, sex, and age of the mice were the same, and the data analysis was single masked. Investigators were not blinded to the group allocation during the experiment and outcome assessment. The number of replicates was indicated in each figure legend. The mean of the technical replicates was used per biological replicate. All statistical tests were justified as appropriate, and the data met the assumptions of the tests. There was an estimate of variation within each group of data.

Data availability

Further information and requests for resources and reagents should be directed to and will be fulfilled by the Lead Contact, Jianfa Zhang (jzhang@mail.njust.edu.cn). This study did not generate new unique materials. All data are contained within the article.

Supporting information—This article contains [supporting information](#).

Author contributions—Yang Zhao, R. C., Yue Zhao, W. G., Y. Y., Z. D., X. X., Z. Wang, and J. Z., conceptualization; Yang Zhao, Yue Zhao, W. G., Y. Y., Z. D., and J. Z., data curation; Yang Zhao, R. C., Y. Y., X. X., Z. Wang, and Z. Wu, formal analysis; J. Z., funding acquisition; Yang Zhao, Yue Zhao, and W. G., investigation; Yang Zhao, R. C., Yue Zhao, W. G., Y. Y., Z. D., X. X., Z. Wang, Z. Wu, and J. Z., methodology; J. Z., project administration; R. C., Yue Zhao, X. X., Z. Wang, Z. Wu, and J. Z. resources; Yang Zhao, Yue Zhao, W. G., Y. Y., Z. D., X. X., and Z. Wu, software; R. C., Z. Wang, Z. Wu, and J. Z., supervision; Yang Zhao, R. C., Yue Zhao, W. G., Y. Y., Z. D., X. X., Z. Wang, and J. Z. validation; Yang Zhao, R. C., W. G., Y. Y., Z. D., X. X., Z. Wang, and Z. Wu, visualization; Yang Zhao, R. C., and J. Z., writing—original draft; Yang Zhao, R. C., Yue Zhao, W. G., Y. Y., Z. D., X. X., Z. Wang, Z. Wu, and J. Z., writing—review and editing.

Funding and additional information—This work was primarily supported by the National Natural Science Foundation of China (NSFC) fund 31861163004 and 31871178 and the Fundamental Research Funds for the Central Universities 30920031102 to J. Z.

Conflict of interest—The authors declare that they have no conflicts of interest with the contents of this article.

Abbreviations—The abbreviations used are: *A1*, *A1* adenosine receptor; *A2a*, *A2a* adenosine receptor; *A2b*, *A2b* adenosine receptor; *A3*, *A3* adenosine receptor; ALT, alanine aminotransferase; AST, aspartate aminotransferase; BUN, blood urea nitrogen; CK-MB, creatine kinase-MB; CRP, C-reactive protein; GK, glucokinase; IL-1 β , interleukin-1; MMP-1, matrix metalloproteinase-1; OPLS-DA, orthogonal projections to latent structures; PCA, principal components analysis; PFK, phosphofructokinase; pH_i, intracellular pH;

SD, standard deviation; T_a , ambient temperature; T_b , core body temperature.

References

1. Heldmaier, G., Ortman, S., and Elvert, R. (2004) Natural hypo-metabolism during hibernation and daily torpor in mammals. *Respir. Physiol. Neurobiol.* **141**, 317–329
2. Drew, K. L., Harris, M. B., LaManna, J. C., Smith, M. A., Zhu, X. W., and Ma, Y. L. (2004) Hypoxia tolerance in mammalian heterotherms. *J. Exp. Biol.* **207**, 3155–3162
3. Sandovici, M., Henning, R. H., Hut, R. A., Strijkstra, A. M., Epema, A. H., van Goor, H., and Deelman, L. E. (2004) Differential regulation of glomerular and interstitial endothelial nitric oxide synthase expression in the kidney of hibernating ground squirrel. *Nitric Oxide* **11**, 194–200
4. Talaie, F., Hylkema, M. N., Bouma, H. R., Boerema, A. S., Strijkstra, A. M., Henning, R. H., and Schmidt, M. (2011) Reversible remodeling of lung tissue during hibernation in the Syrian hamster. *J. Exp. Biol.* **214**, 1276–1282
5. Rouble, A. N., Hefler, J., Mamady, H., Storey, K. B., and Tessier, S. N. (2013) Anti-apoptotic signaling as a cytoprotective mechanism in mammalian hibernation. *PeerJ* **1**, e29
6. Tøien, Ø., Drew, K., Chao, M., and Rice, M. (2001) Ascorbate dynamics and oxygen consumption during arousal from hibernation in Arctic ground squirrels. *Am. J. Physiol. Regul. Integr. Comp. Physiol.* **281**, R572–R583
7. Bouma, H. R., Carey, H. V., and Kroese, F. G. (2010) Hibernation: The immune system at rest? *J. Leukoc. Biol.* **88**, 619–624
8. Aslami, H., and Juffermans, N. P. (2010) Induction of a hypometabolic state during critical illness - a new concept in the ICU? *Neth. J. Med.* **68**, 190–198
9. Asfar, P., and Radermacher, P. (2015) Drug-induced “suspended animation”: Can a dream become true? *Crit. Care Med.* **43**, 1528–1530
10. Ruf, T., and Geiser, F. (2015) Daily torpor and hibernation in birds and mammals. *Biol. Rev. Camb. Philos. Soc.* **90**, 891–926
11. Geiser, F., and Ruf, T. (1995) Hibernation versus daily torpor in mammals and birds: Physiological variables and classification of torpor patterns. *Physiol. Zoology* **68**, 935–966
12. Hartmann, C., Nussbaum, B., Calzia, E., Radermacher, P., and Wepler, M. (2017) Gaseous mediators and mitochondrial function: The future of pharmacologically induced suspended animation? *Front. Physiol.* **8**, 691
13. Blackstone, E., Morrison, M., and Roth, M. B. (2005) H2S induces a suspended animation-like state in mice. *Science* **308**, 518
14. Yalamanchili, C., and Smith, M. D. (2008) Acute hydrogen sulfide toxicity due to sewer gas exposure. *Am. J. Emerg. Med.* **26**, 518.e5–518.e7
15. Daniels, I. S., Zhang, J., O'brien, W. G., Tao, Z., Miki, T., Zhao, Z., Blackburn, M. R., and Lee, C. C. (2010) A role of erythrocytes in adenosine monophosphate initiation of hypometabolism in mammals. *J. Biol. Chem.* **285**, 20716–20723
16. Jinka, T. R., Tøien, Ø., and Drew, K. L. (2011) Season primes the brain in an arctic hibernator to facilitate entrance into torpor mediated by adenosine A(1) receptors. *J. Neurosci.* **31**, 10752–10758
17. Stamper, J. L., Dark, J., and Zucker, I. (1999) Photoperiod modulates torpor and food intake in Siberian hamsters challenged with metabolic inhibitors. *Physiol. Behav.* **66**, 113–118
18. Bouma, H. R., Verhaag, E. M., Otis, J. P., Heldmaier, G., Swoap, S. J., Strijkstra, A. M., Henning, R. H., and Carey, H. V. (2012) Induction of torpor: Mimicking natural metabolic suppression for biomedical applications. *J. Cell. Physiol.* **227**, 1285–1290
19. Buck, M. J., Squire, T. L., and Andrews, M. T. (2002) Coordinate expression of the PDK4 gene: A means of regulating fuel selection in a hibernating mammal. *Physiol. Genomics* **8**, 5–13
20. Castex, C., Tahri, A., Hoo-Paris, R., and Sutter, B. C. (1987) Glucose oxidation by adipose tissue of the edible dormouse (*Glis glis*) during hibernation and arousal: Effect of insulin. *Comp. Biochem. Physiol. A Comp. Physiol.* **88**, 33–36
21. Hoo-Paris, R., Castex, C., and Sutter, B. C. (1978) Plasma glucose and insulin in the hibernating hedgehog. *Diabete Metab.* **4**, 13–18
22. Balasubramanian, T. (2003) Uric acid or 1-methyl uric acid in the urinary bladder increases serum glucose, insulin, true triglyceride, and total cholesterol levels in Wistar rats. *ScientificWorldJournal* **3**, 930–936
23. Robin, J.-P., Boucontet, L., Chillet, P., and Groscolas, R. (1998) Behavioral changes in fasting emperor penguins: Evidence for a “refeeding signal” linked to a metabolic shift. *Am. J. Physiol. Regul. Integr. Comp. Physiol.* **274**, R746–R753
24. Jenni, L., Jenni-Eiermann, S., Spina, F., and Schwabl, H. (2000) Regulation of protein breakdown and adrenocortical response to stress in birds during migratory flight. *Am. J. Physiol. Regul. Integr. Comp. Physiol.* **278**, R1182–R1189
25. Wilhelmi de Toledo, F., Grundler, F., Goutzourelas, N., Tekos, F., Vassi, E., Mesnage, R., and Kouretas, D. (2020) Influence of long-term fasting on blood redox status in humans. *Antioxidants* **9**, 496
26. Carey, H. V., Andrews, M. T., and Martin, S. L. (2003) Mammalian hibernation: Cellular and molecular responses to depressed metabolism and low temperature. *Physiol. Rev.* **83**, 1153–1181
27. Wu, C. W., Biggar, K. K., and Storey, K. B. (2013) Biochemical adaptations of mammalian hibernation: Exploring squirrels as a perspective model for naturally induced reversible insulin resistance. *Braz. J. Med. Biol. Res.* **46**, 1–13
28. Geiser, F. (2013) Hibernation. *Curr. Biol.* **23**, R188–193
29. Storey, K. B. (2010) Out cold: Biochemical regulation of mammalian hibernation - a mini-review. *Gerontology* **56**, 220–230
30. Chung, D., Lloyd, G. P., Thomas, R. H., Guglielmo, C. G., and Staples, J. F. (2011) Mitochondrial respiration and succinate dehydrogenase are suppressed early during entrance into a hibernation bout, but membrane remodeling is only transient. *J. Comp. Physiol. B* **181**, 699–711
31. Heim, A. B., Chung, D., Florant, G. L., and Chicco, A. J. (2017) Tissue-specific seasonal changes in mitochondrial function of a mammalian hibernator. *Am. J. Physiol. Regul. Integr. Comp. Physiol.* **313**, R180–r190
32. Holeček, M. (2020) Why are branched-chain amino acids increased in starvation and diabetes? *Nutrients* **12**, 3087
33. Fillmore, N., Mori, J., and Lopaschuk, G. D. (2014) Mitochondrial fatty acid oxidation alterations in heart failure, ischaemic heart disease and diabetic cardiomyopathy. *Br. J. Pharmacol.* **171**, 2080–2090
34. Dudzinska, W. (2014) Purine nucleotides and their metabolites in patients with type 1 and 2 diabetes mellitus. *J. Biomed. Sci. Engg.* **7**, 38–44
35. Fiehn, O., Garvey, W. T., Newman, J. W., Lok, K. H., Hoppel, C. L., and Adams, S. H. (2010) Plasma metabolomic profiles reflective of glucose homeostasis in non-diabetic and type 2 diabetic obese African-American women. *PLoS One* **5**, e15234
36. Dehghan, A., van Hoek, M., Sijbrands, E. J., Hofman, A., and Witteman, J. C. (2008) High serum uric acid as a novel risk factor for type 2 diabetes. *Diabetes Care* **31**, 361–362
37. Kodama, S., Saito, K., Yachi, Y., Asumi, M., Sugawara, A., Totsuka, K., Saito, A., and Sone, H. (2009) Association between serum uric acid and development of type 2 diabetes. *Diabetes Care* **32**, 1737–1742
38. Sluijs, I., Holmes, M. V., van der Schouw, Y. T., Beulens, J. W., Asselbergs, F. W., Huerta, J. M., Palmer, T. M., Arriola, L., Balkau, B., Barriarte, A., Boeing, H., Clavel-Chapelon, F., Fagherazzi, G., Franks, P. W., Gavrilu, D., et al. (2015) A Mendelian randomization study of circulating uric acid and type 2 diabetes. *Diabetes* **64**, 3028–3036
39. Soto, M., Orliaguet, L., Reyzer, M. L., Manier, M. L., Caprioli, R. M., and Kahn, C. R. (2018) Pyruvate induces torpor in obese mice. *Proc. Natl. Acad. Sci. U. S. A.* **115**, 810–815
40. Tschirner, S. K., Gutzki, F., Schneider, E. H., Seifert, R., and Kaever, V. (2016) Neurotransmitter and their metabolite concentrations in different areas of the HPRT knockout mouse brain. *J. Neurol. Sci.* **365**, 169–174
41. Jinnah, H., Wojcik, B., Hunt, M., Narang, N., Lee, K., Goldstein, M., Wamsley, J., Langlais, P., and Friedmann, T. (1994) Dopamine deficiency in a genetic mouse model of Lesch-Nyhan disease. *J. Neurosci.* **14**, 1164–1175
42. Liu, C., Lee, C. Y., Asher, G., Cao, L., Terakoshi, Y., Cao, P., Kobayakawa, R., Kobayakawa, K., Sakurai, K., and Liu, Q. (2021) Posterior subthalamic

Diabetic mice enter hibernation-like suspended animation

- nucleus (PSTh) mediates innate fear-associated hypothermia in mice. *Nat. Commun.* **12**, 2648
43. Hrvatin, S., Sun, S., Wilcox, O. F., Yao, H., Lavin-Peter, A. J., Cicconet, M., Assad, E. G., Palmer, M. E., Aronson, S., Banks, A. S., Griffith, E. C., and Greenberg, M. E. (2020) Neurons that regulate mouse torpor. *Nature* **583**, 115–121
 44. Takahashi, T. M., Sunagawa, G. A., Soya, S., Abe, M., Sakurai, K., Ishikawa, K., Yanagisawa, M., Hama, H., Hasegawa, E., Miyawaki, A., Sakimura, K., Takahashi, M., and Sakurai, T. (2020) A discrete neuronal circuit induces a hibernation-like state in rodents. *Nature* **583**, 109–114
 45. Wu, X. W., Lee, C. C., Muzny, D. M., and Caskey, C. T. (1989) Urate oxidase: Primary structure and evolutionary implications. *Proc. Natl. Acad. Sci. U. S. A.* **86**, 9412–9416
 46. Kakino, J., Sato, R., and Naito, Y. (1998) Purine metabolism of uric acid urolithiasis induced in newborn piglets. *J. Vet. Med. Sci.* **60**, 203–206
 47. Dorion, D., Zhong, A., Chiu, C., Forrest, C. R., Boyd, B., and Pang, C. Y. (1993) Role of xanthine oxidase in reperfusion injury of ischemic skeletal muscles in the pig and human. *J. Appl. Physiol.* **75**, 246–255
 48. Podzuweit, T., Braun, W., Müller, A., and Schaper, W. (1987) Arrhythmias and infarction in the ischemic pig heart are not mediated by xanthine oxidase-derived free oxygen radicals. *Basic Res. Cardiol.* **82**, 493–505
 49. Janssen, M., van der Meer, P., and de Jong, J. W. (1993) Antioxidant defences in rat, pig, Guinea pig, and human hearts: Comparison with xanthine oxidoreductase activity. *Cardiovasc. Res.* **27**, 2052–2057
 50. Zhang, D., Liu, H., Luo, P., and Li, Y. (2018) Production inhibition and excretion promotion of urate by Fucoidan from *Laminaria japonica* in adenine-induced hyperuricemic mice. *Mar. Drugs* **16**, 472
 51. Pyo, Y. H., Hwang, J. Y., and Seong, K. S. (2018) Hypouricemic and antioxidant effects of soy vinegar extracts in hyperuricemic mice. *J. Med. Food* **21**, 1299–1305
 52. Wang, Y., Zhu, J. X., Kong, L. D., Yang, C., Cheng, C. H., and Zhang, X. (2004) Administration of procyanidins from grape seeds reduces serum uric acid levels and decreases hepatic xanthine dehydrogenase/oxidase activities in oxonate-treated mice. *Basic Clin. Pharmacol. Toxicol.* **94**, 232–237
 53. Lu, J., Dalbeth, N., and Yin, H. (2019) Mouse models for human hyperuricaemia: A critical review. *Nat. Rev. Rheumatol.* **15**, 413–426
 54. Nelson, R. A., Wahner, H. W., Jones, J. D., Ellefson, R. D., and Zollman, P. E. (1973) Metabolism of bears before, during, and after winter sleep. *Am. J. Physiol.* **224**, 491–496
 55. Dutton, C. J., and Taylor, P. (2003) A comparison between pre- and posthibernation morphometry, hematology, and blood chemistry in viperid snakes. *J. Zoo Wildl. Med.* **34**, 53–58
 56. Polderman, K. H. (2009) Mechanisms of action, physiological effects, and complications of hypothermia. *Crit. Care Med.* **37**, S186–202
 57. Yong, T., Chen, S., Xie, Y., Shuai, O., Li, X., Chen, D., Su, J., Jiao, C., and Liang, Y. (2018) Hypouricemic effects of extracts from *Agrocybe aegerita* on hyperuricemic mice and virtual prediction of bioactives by molecular docking. *Front. Pharmacol.* **9**, 498
 58. Knudsen, T. B., Winters, R. S., Otey, S. K., Blackburn, M. R., Airhart, M. J., Church, J. K., and Skalko, R. G. (1992) Effects of (R)-deoxycoformycin (pentostatin) on intrauterine nucleoside catabolism and embryo viability in the pregnant mouse. *Teratology* **45**, 91–103
 59. Smolenski, R. T., Lachno, D. R., Ledingham, S. J. M., and Yacoub, M. H. (1990) Determination of sixteen nucleotides, nucleosides and bases using high-performance liquid chromatography and its application to the study of purine metabolism in hearts for transplantation. *J. Chromatogr.* **527**, 414–420
 60. Zou, C., Wang, Y., and Shen, Z. (2005) 2-NBDG as a fluorescent indicator for direct glucose uptake measurement. *J. Biochem. Biophys. Methods* **64**, 207–215
 61. Humez, S., Monet, M., van Coppenolle, F., Delcourt, P., and Prevarskaya, N. (2004) The role of intracellular pH in cell growth arrest induced by ATP. *Am. J. Physiol. Cell Physiol.* **287**, C1733–1746
 62. Schlatter, E., Ankorina-Stark, I., Haxelmans, S., and Hohage, H. (1997) Moxonidine inhibits Na⁺/H⁺ exchange in proximal tubule cells and cortical collecting duct. *Kidney Int.* **52**, 454–459
 63. Uthman, L., Baartscheer, A., Bleijlevens, B., Schumacher, C. A., Fiolet, J. W. T., Koeman, A., Jancev, M., Hollmann, M. W., Weber, N. C., Coronel, R., and Zuurbier, C. J. (2018) Class effects of SGLT2 inhibitors in mouse cardiomyocytes and hearts: Inhibition of Na⁽⁺⁾/H⁽⁺⁾ exchanger, lowering of cytosolic Na⁽⁺⁾ and vasodilation. *Diabetologia* **61**, 722–726
 64. Beckonert, O., Keun, H. C., Ebbels, T. M., Bundy, J., Holmes, E., Lindon, J. C., and Nicholson, J. K. (2007) Metabolic profiling, metabolomic and metabonomic procedures for NMR spectroscopy of urine, plasma, serum and tissue extracts. *Nat. Protoc.* **2**, 2692–2703
 65. Dieterle, F., Schlotterbeck, G., Ross, A., Niederhauser, U., and Senn, H. (2006) Application of metabolomics in a compound ranking study in early drug development revealing drug-induced excretion of choline into urine. *Chem. Res. Toxicol.* **19**, 1175–1181